

Large-scale and Efficient Texture Mapping Algorithm via Loopy Belief Propagation

Xiao Ling, Rongjun Qin, *Senior Member, IEEE*

Abstract—Texture mapping as a fundamental task in 3D modeling has been well established for well-acquired aerial assets under consistent illumination, yet it remains a challenge when it is scaled to large datasets with images under varying views and illuminations. A well-performed texture mapping algorithm must be able to efficiently select views, fuse and map textures from these views to mesh models, at the same time, achieve consistent radiometry over the entire model. Existing approaches achieve efficiency either by limiting the number of images to one view per face, or simplifying global inferences to only achieve local color consistency. In this paper, we break this tie by proposing a novel and efficient texture mapping framework that allows the use of multiple views of texture per face, at the same time to achieve global color consistency. The proposed method leverages a loopy belief propagation algorithm to perform an efficient and global-level probabilistic inferences to rank candidate views per face, which enables face-level multi-view texture fusion and blending. The texture fusion algorithm, being non-parametric, brings another advantage over typical parametric post color correction methods, due to its improved robustness to non-linear illumination differences. The experiments on three different types of datasets (i.e. satellite dataset, unmanned-aerial vehicle dataset and close-range dataset) show that the proposed method has produced visually pleasant and texturally consistent results in all scenarios, with an added advantage of consuming less running time as compared to the state of the art methods, especially for large-scale dataset such as satellite-derived models.

Index Terms—texture mapping, belief propagation, multiple labels, image blending.

I. INTRODUCTION

TEXTURE mapping (TM) is defined as assigning textural materials to 3D geometry (meshes or polyhedral models), such that it is visually consistent and contextually correct. It serves as a fundamental step for almost all 3D modeling pipelines, and this is especially becoming a standard step in 3D mesh modeling using well-acquired aerial assets [1]–[3]. However, this is still a challenging problem when such a task is scaled to a very large dataset, or in general scenarios where the

Xiao Ling is with Geospatial Data Analytics Laboratory, The Ohio State University, 218B Bolz Hall, 2036 Neil Avenue, Columbus, OH 43210, USA, and also with Department of Civil, Environmental and Geodetic Engineering, The Ohio State University, 218B Bolz Hall, 2036 Neil Avenue, Columbus, OH 43210, USA, also with College of Astronautics, Nanjing University Of Aeronautics And Astronautics, 29 Jiangjun Avenue, Jiangning District, Nanjing, Jiangsu 211106, China. (email: xlingsky@nuaa.edu.cn)

Rongjun Qin is with Geospatial Data Analytics Laboratory, The Ohio State University, 218B Bolz Hall, 2036 Neil Avenue, Columbus, OH 43210, USA, and also with Department of Civil, Environmental and Geodetic Engineering, The Ohio State University, 218B Bolz Hall, 2036 Neil Avenue, Columbus, OH 43210, USA, also with Department of Electrical and Computer Engineering, The Ohio State University, 205 Dreese Lab, 2036 Neil Avenue, Columbus, OH 43210, USA, also with Translational Data Analytics Institute, The Ohio State University. (email: qin.324@osu.edu, corresponding author)

image size is large and images are captured under drastically different lighting conditions. For example, TM using multi-view satellite images [4], [5] possesses both challenges. On the one hand, performing TM on mesh models at the city scale requires the TM algorithms to balance both memory and computational efficiency; on the other hand, these multi-images are often collected at different times/seasons under various illumination. Such challenges similarly exist when sources of textures are coming from different sensors.

There exists a large number of well-performed TM algorithms in both the computer graphics and computer vision domains [6]–[8], aiming at image selection, and color balancing among neighboring triangles/faces locally, and color/lighting consistency among the entire 3D model. Oftentimes, the process of performing global color balancing requires highly efficient algorithms. These algorithms, however, come at the expense of sacrificing the used information among all eligible texture materials from different viewpoints. For example, the classic graph-cut based image selection algorithm used in [6], [7], considered selecting a single view for each face/triangle, while attributed solutions of addressing illumination disparities among different views solely to post-correction algorithms, which by concept, is limited by the capacity of the correction models; for instance, major post-correction models utilize either a bias term or at maximum a linear correction model, which are incapable of addressing non-linear color differences that are otherwise very common in practice. On the other hand, the very classic, view-dependent TM scheme [9], considers a fusion of multiple image textures seen by a single face/triangle in the 3D object, using weighting strategies based on the viewing angle, the level of coverage, etc. However, since the fusion is carried out independently for each triangle/face in the 3D model, this, in contrast, sacrifices the global color consistencies among neighboring faces and the overall 3D model, for two reasons: 1) the fusion for individual triangles/faces will consume a large number of computation power (considering models with millions of triangle faces and more); 2) the fused image lost its belongingness to a particular source view, thus is unable to exploit the level of color consistencies among neighboring triangle/faces as if they were from a single image. If these two seemingly conflicting schemes can be leveraged under the same TM framework, it will facilitate TM algorithms that enjoy the pros of existing TM methods, to be thus both accurate and efficient.

In this paper, we propose a novel texture mapping framework to achieve both efficiency and accuracy as to address the aforementioned limitations for TM: instead of fusing the multiple image textures at the first place, we consider ranking

these multiple image textures at the triangle level, which leverages a number of cues to yield consistent textures and only fuse the top few. The ranking of image texture for each triangle is obtained by utilizing not only local cues, such as the viewing angles, and coverage of the image, but also global cues such as the color resemblance of image texture candidates and consistency in their source image ID for neighboring triangles/faces. This framework will additionally allow optional post-correction as needed, or directly involve these multiple image textures in the post-correction process. In other words, our method, instead of selecting a single view, preserves multiple image textures prior to fusion and post-correction, which will, on one hand, allow global inferences to select multiple image texture candidates, and on the other hand, provide the flexibility to perform non-parametric color corrections to accommodate various levels of illumination differences among different images. We found the solution of our proposed method can be achieved through a belief-propagation framework [10], owing to its unique advantage in allowing global probabilistic inferences through information passing for multiple variables (here referred to as multiple image texture candidates), as compared to graph-cut solutions [11], [12] that only offer a deterministic solution as the cut. We carry out experiments using various datasets including satellite, aerial and close-range images and models using our method and compared it with the state-of-the-arts (SOTAs) and have shown unique advantages in various case scenarios. As for example, because our approach allows reserving multiple texture candidates, it is able to generate consistent and visually pleasing textures for façades in high-altitude mapping cases (i.e., satellite images) despite that façade information is rather limited.

The rest of this paper is organized as follows: **Section II** presents a literature survey related to existing methods in TM for 3D modeling. **Section III** describes our proposed algorithms and especially our critical additions to the existing literature. Experimental results and comparative studies on three different datasets are presented in **Section IV**. **Section V** concludes this paper by analyzing the advantages and drawbacks of our methodology that inform our planned future works.

II. RELATED WORK

Given a set of images with poses and a 3D geometric model (e.g. meshes or polyhedral models), a plain version of a TM algorithm transverses all the faces, and for each face, it selects a visible view and projects its valid portion to the face as an assigned texture material. This plain version of TM algorithm apparently drives two practical challenges in order to achieve optimized results: first, how to select the view(s) among multiple (often a large number of) visible views to maximize texture quality; second, texture materials from different source views on neighboring faces inevitably result in inconsistent texture transitions, and how to correct such texture inconsistency across the entire model. These two challenges are correlated, as consistent texture transitions may serve as a criterion for view selection, e.g., one can purposely select

views to minimize inconsistent source views for textures of neighboring views. Therefore, the TM has became a multi-complex problem that requires solutions to be systematic, robust and efficient.

Existing approaches either focus on addressing one of the challenges, or both following a sequential order. Generally, we categorize them into two classes: 1) the blending-based methods and 2) the Markov Random Field (MRF) based TM framework. The former mainly focuses on addressing the second challenge by exploiting weight fusion of all possible image textures [9], to achieve texture homogeneity across the entire model, and the latter, however, starts with view selection by modeling views per face as a random variable in a Markov Random Field (MRF) [13], thus to allow the consistency constraints to be imposed on neighboring faces to achieve a global texture consistency optimum [7], [14]. Such an approach is often followed by an optional post-correction of the remaining inconsistent textures [6], [7].

A. Blending-based Methods

The blending-based approaches [2], [9], [15] consider all visible views per face, and project all input images onto the surface of the 3D model using the camera pose and then blend/fuse them. The blending is achieved either with equal weights or with other image quality indicators, such as resolution, viewing angles etc., to achieve a consistent texture map. The underlying concept is that such a weighted sum inherently builds a spatially smooth function with respect to the image textures, and as a result the blended image averages out potential conflicting illuminations of different images, to achieve smooth transitions across neighboring faces. Such blending methods, called alpha blending with many of its variants [16]–[18]. Specifically, a commonly used approach, called distance transform based alpha blending [19], is to firstly compute the distance to the nearest invalid pixel for each pixel on an image to generate a distance map and then fuse all views together with distance maps as weights, which inherently assume the image texture resides in the center of the image with higher weights and vice versa.

This type of approach, however, has some critical drawbacks. First, the fact of fusing all visible views means tolerating all potential sources of errors which are not easily accountable by weighted blending, such as drastic image resolution difference, camera pose errors, strong illumination differences etc., thus often result in blurred texture materials, reduced textured resolution and ghosting artifacts. Second, although this type of approach enjoys the benefit of memory efficiency due to that it is a local method (each face is processed independently), blending all visible views also means to tolerate notoriously heavy computation when the number of views is large (in the order of tens to hundreds), leading to sometimes unbearable waiting time. Third, this type of approach being local, although produces locally smooth texture transitions, will not accommodate global illumination differences that are spatially distant. It should be noted there are approaches to deal with the first drawback by introducing more advanced approaches than simple weighted blending. For

example, Bi et al. [8] improved the blending method by synthesizing aligned images from input images even with inaccurate camera poses by proposing a patch-based optimization system to avoid ghosting and blurring artifacts in the result. Despite the performance gain, this approach with an added layer of complexity will only further increase the computation when dealing with a large number of views. Thus, it is only suitable for close-range and small-range models, such as indoor scenes and small objects.

B. MRF-based Texture Mapping framework

Lempitsky and Ivanov [7] first proposed the MRF based TM framework to select an optimal view for each mesh face. Based on their work, other similar works [6], [16], [20]–[22] focused on improving the terms of the energy function or modifying them to adapt to different scene contexts, such as for RGB-D (depth) data. Among these methods, [6] plays an important role for large-scale TM by introducing high performance data term and smooth term as well as a post-correction on texture colors with a two-step adjustment (i.e. global seam leveling, followed by a local adjustment with Poisson editing [23]) to achieve high efficiency and uniform color. It is also one of the most well-engineered and open-source methods adopted by the well-known OpenMVS package [24]. Therefore, it consistently serves as a baseline approach for comparison, and is still presented as one of the top approaches for dealing with practical TM problems with large datasets. However, this type of approach still suffers from a few drawbacks: 1) The fact of only selecting a single view per face will inevitably result in sub-optimal texture selection at certain faces. For example, the faces of building roofs and façades are topologically connected and ideally chosen the same view for both will avoid seamlines between two faces, while the same view is apparently not ideal to provide the best textural coverage, as roof faces favor nadir images while façade faces favor oblique views. Thus, in theory, it is very difficult to design a view selection algorithm that accommodates multiple objectives. 2) the fact of using only one view will inevitably encounter scenarios where one needs to consider post-correction of inconsistent texture colors at faces which are beyond what a single view can cover. Additionally, the post-correction of inconsistent textures is essentially a global operation, which requires heavy computation even with simple linear (or bias) corrections. In Waechter et al. [6], this was performed two-step method to correct complex color inconsistencies, while it takes a long running time, is still insufficiently accurate to yield realistic colors, e.g. issues of discoloration affected by shadowed façades connected with well illuminated roof tops.

MRF Solver: The MRF framework embedding various constraints, such as number of views, coverages and incidence angles etc., can be solved by various classes of solvers such as Loopy Belief Propagation (LBP), Graph Cuts (GC) and Convergent Tree Reweighted Message Passing (TRW-S) [25]. According to Lempitsky and Ivanov [7], GC solver demonstrates the best performance, which was further used by other similar works [6], [16], [21], [22]. As a result, the fact of these methods only returning a single view per face,

is limited by the GC solver, because it only provides a final labeling (which view to choose) subject to minimizing the formulated energy function.

Post-correction of inconsistent textures: An example of the post-correction method [7], computed globally optimal luminance correction as a bias term added to each vertex of faces, with the goal to minimize the luminance differences per vertex at seams to allow smooth color transition. Waechter et al. [6] further improved it by adjusting the color along the seams via Poisson editing to allow smoother transitions across neighboring faces. The solver of these bias terms will result in a large and exponentially growing sparse matrix with the number of faces, facing both computation and numerical stability challenges.

However, GC cannot be parallelized easily due to the graph's irregular structure, while the LBP solver can be fully parallelized, which implies the LBP solver may overtake the GC solver on multi-core machines for performance. More importantly, the LBP solver is able to return the costs of views for each mesh face, so that not just one view per face but top N views can be assigned to a face at once.

C. Considerations leading to the proposed method

While the MRF framework is regarded as a popular approach, one fundamental bottleneck is that it is limited to selecting one view per face, which leads to sub-optimal views that cannot accommodate multiple objectives. If more views are selected under the MRF framework, it may allow flexibility to enable blending methods on these selected views and thus to achieve seamless texture transitions without complex post-correction methods. We consider the major hurdle of this “one view” limitation is caused by the use of “GC” solver, although it is regarded as the most accurate (reported by [7]). We therefore leverage this by using the LBP solver to perform the MRF optimization, since it allows explicit probabilistic inferences for the random variable, which we can use a cue to design more flexible constraints to achieve multiple objectives, as well as return multiple candidates of views based on the explicit probability distributions for each potential view candidates. Therefore, the idea here is to construct an energy function using constraints such as view consistency, coverage, viewing angles, etc., to maximize the quality of the image candidate; retrieve the probability distribution of potential views via a LBP solver, rank them to reflect the multiple objectives, and only blend the top N views that fulfill the objectives to achieve smooth texture transition (without including bad texture that pollutes the blended image). This will automatically achieve global color consistency (due to the MRF frame), and local smooth texture transition (due to per face blending), without the possible need to perform post-correction, which was supposed to alleviate color inconsistencies due to the lack of blending in MRF frameworks.

III. OUR PROPOSED APPROACH

Following our considerations as mentioned in **Section II-C**, our proposed work follows the Markov Random Field (MRF) based TM framework, which constructs a global optimization

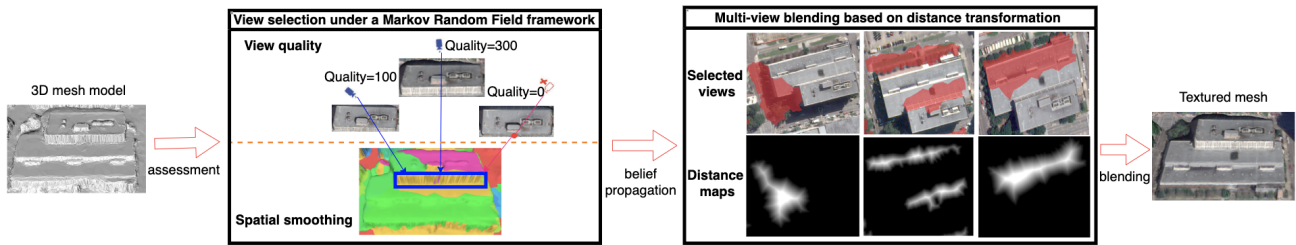


Fig. 1. The proposed workflow. Given a 3D mesh model and the corresponding oriented images, the qualities of views are firstly computed as visibility, projected area and color-consistency for each face, and then all these terms are formulated into a MRF energy function solved by LBP, which returns top N views to each face. A multi-view blending algorithm is finally applied to yield the seamless high-quality texture.

involving data terms and smooth terms to balance the quality per view and the severity of seams between texture patches. As shown in **Fig. 1**, given the 3D mesh and its associated images with known orientation parameters, the qualities of views are computed in terms of visibility, projected area and color-consistency for each face, and then all these terms are packed into a pairwise MRF energy formulation solved by Loopy Belief Propagation (LBP) to assign top N best views to each face, finally a multi-view blending algorithm based on distance map [26] is applied to yield the texture with uniform color. Details of those steps are introduced in the following sub-sections.

A. Multi-objectives for view quality assessment

To evaluate the quality of views when texturing a face, we first select the visible views (by an occlusion detector), and then employ quality indicators with the following considerations: 1) the selected views should contain maximal texture details, 2) the selected view textures should have minimal geometrical distortions, and 3) the selected views should be “popular” to warrant consistent colors among neighboring faces. The first two considerations are coherent, and can be well-represented by the resolution of the projected areas [16], [27], [28], meaning the number of pixels in the projected footprint of a triangle face in a view, because this inherently implies a smaller incidence angle leading to less distorted texture, and more pixels per unit area leading to more textural details. “Popular” views refer to the fact of view selecting being smooth, meaning that neighboring faces select views in the color-consistent set (i.e. the majority), consistent texture illumination can be achieved as they came from the majority. In summary, the following quality indicators are considered when evaluating a view (visual illustration can be found in **Fig. 2**)

(1) Visibility. Occluded views (non-visible views) cannot be considered as view candidates. Here, to accommodate generic camera models (i.e. frame camera model, linear-array or parametric models (RPC (Rational Polynomial Coefficient)-based)), we use a simple z-buffer algorithm [29] that renders depth values from the geometry to potentially candidate views and only views identified as visible will be considered. Such a rendering scheme can be hardware accelerated and present an efficient means to filter out invisible views.

(2) Resolution of the projected area S. As described above, a larger projection area implies better incidence angle

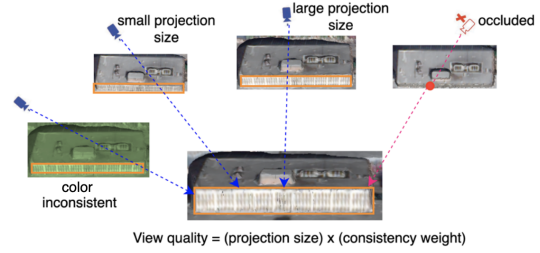


Fig. 2. Illustration for view quality assessment. All occluded views are eliminated firstly. The resolution of the projected area (i.e. the projection size) is used as a quality indicator since a larger projection size implies small incidence angle leading to less distorted texture and higher image resolution leading to more textural details. Color inconsistency is another quality indicator to warrant consistent texture illumination among neighboring faces.

and higher image resolution. Thus, the projection area of a face on a view would be an efficient way to judge view quality. Although, as argued in Waechter's paper [6], optimizing the projection size may lead to out-of-focus blur as it tends to select views whose image plane are close to the object. This is, however, only problematic in extremely close-range applications, which can be easily leveraged by other constraints (e.g. the distance between the perspective center to the object's surface).

(3) Color consistency ω . To minimize the inconsistency of final texture charts, views with consistent colors should be given higher weights of consideration. On the contrary, views with inconsistent colors against the majority (e.g. some shadowed textures) should be punished. Here, among all view candidates, we tend to first compute the mean brightness (color) of these views and give higher weight to those close to the mean and lower to drastically different ones. The mean color is computed via a modified mean-shift algorithm [6], computed as: given a list of views for a specific face,

- 1) Compute the face projection's mean color c_i for all visible pixels on view l_i .
- 2) Compute mean μ and covariance matrix Σ of all views' mean color c_i .
- 3) Evaluate the multi-variate Gaussian function $e^{-\frac{(c_i - \mu)^T \Sigma (c_i - \mu)}{2}}$ for each view l_i .
- 4) Eliminate the views whose function value is below a threshold (we use 0.006 for 8-bit image).
- 5) Repeat 3.-4. for 10 iterations or until the inversion of Σ becomes stable, i.e. all entries of Σ drop below 10^{-5} ,

or the number of inliers is less than 4.

6) Compute the Gaussian function value for each view l_i as its weight of view quality to raise up the probability for color-consistent views in the following view selection procedure.

In summary, the final score of view quality Q of a view l_i for a specific face F_i is computed by a product of face projection's size $S(F_i, l_i)$ (i.e. the number of visible pixels within the projected region) and its color consistency's weight $\omega(F_i, l_i)$ (see **Equation 1**), to prevent the view with less visible pixels or larger color difference being selected.

$$Q(F_i, l_i) = \omega(F_i, l_i)S(F_i, l_i) \quad (1)$$

B. View selection under a Markov Random Field framework

The per-face view quality indicator as described in **Section III-A** does not consider spatial smoothness, because a single/linear quality indicator for a face is insufficient to model the complex correlation between view quality and its potential smoothness in connection to its neighbors. It is possible that spatial smoothness contradicts the view quality, and on occasions, the selection will need to sacrifice the view quality (higher texture details), in order to achieve smooth color transitions. Therefore, we consider optimizing the view selection through a Markovian process using a MRF Framework, which allows the consideration of these quality indicators as well as view consistencies across spatially connected faces. Unlike typical MRF solvers for view selection [7] which produce a single and finalized view per face, the aim of this proposed MRF process is to allow view indicator inferences to obtain top view candidates per face for texture fusion. The MRF energy function is formulated as follows:

$$E(l) = \sum_{F_i \in \mathbb{N}_f} E_{data}(F_i, l_i) + \sum_{(F_i, F_j) \in \mathbb{N}_e} E_{smooth}(F_i, F_j, l_i, l_j) \quad (2)$$

where, l_i denotes the view assigned to a mesh face F_i , \mathbb{N}_f is the mesh face set and \mathbb{N}_e is the mesh edge set. The first term is the data term E_{data} which prefers views with high quality for a face and the second term is the smoothness term E_{smooth} which punishes inconsistent labels between neighboring faces which share a common edge. Details about these terms are further given below.

- 1) **Data term:** For the reasons described in **Section III-A**, the cost $E_{data}(F_i, l_i)$ for a view l_i assigned to a mesh face F_i is computed as $E_{data}(F_i, l_i) = Q(F_i, l_i)$, here $Q(F_i, l_i)$ is the score of view quality computed from **Equation 1**.
- 2) **Smoothness term:** The Potts model: $E_{smooth} = [l_i \neq l_j]$ ($[\cdot]$ is the Iverson bracket) is used as a smoothness term to favor a consistent label between neighboring mesh faces. This also prefers compact patches and is extremely fast to compute.

The energy minimization problem (**Equation 2**) can be solved by many algorithms, e.g. LBP, α -expansion GC and Convergent Tree Reweighted Message Passing (TRW-S). However, for GC or TRW-S as typical solvers, only

return a single label, which will inevitably cause seamlines at the edges shared by two faces with different labels, thus computationally expensive post-correction is necessary, such as a local adjustment with Poisson editing used in Waechter et al. [6]. Here we consider a simple extension to avoid this computation: instead of assigning the best view for each face, we reserve the top N (we used 3 in this work) views after the inference and perform a simple and weighted linear blending. Therefore, we apply a LBP solver to resolve the energy function (**Equation 2**), and rank the candidates based on the cost volumes for each possible view, which provides much more flexibility to blend textures to potentially avoid seamlines. The diversity of views is depicted in **Fig. 3 (left)**, with the right image of **Fig. 3** showing the seamlines if only a single (and the best view is selected), and the blended result is shown in **Fig. 4(d)**. Since the data term gives lower costs to the majority of views and the smoothness term prefers a consistent label between neighboring faces, the color difference of the top N candidates for a face will drop into a fine level and the view candidates for the neighboring faces will have common elements as well after optimizing **Equation 2**. Details of the LBP solver are as follows:

Given a pair of neighboring nodes (i.e. two mesh faces F_i and F_j with a common edge), the directed message m_{F_i, F_j} from F_i to F_j , which is initialized to 1, is updated by considering all messages flowing into F_i (except for message from F_j) via **Equation 3**, where $\mathbb{N}(F_i) \setminus F_j$ is the set of neighboring faces except F_j for F_i , the cost of each view l_i for face F_i are computed from **Equation 4** and the smallest cost is taken as its selected view, this procedure iterates for a fixed number of iterations (e.g. 50 in our experiments) or until **Equation 2** reaches the minimum, and views with the smallest cost for each face are taken as final solutions. In practice, one usually normalizes the messages m_{F_i, F_j} to sum to 1, so that $\sum_{l_j} m_{F_i, F_j}(l_j) = 1$, in every iteration for numerical stability. Both messages (**Equation 3**) and costs (**Equation 4**) computation are parallelizable and have been fully parallelized in our implementation.

$$m_{F_i, F_j}^{new}(l_j) = \sum_{l_i} \left(E_{data}(F_i, l_i) E_{smooth}(F_i, F_j, l_i, l_j) \prod_{F_k \in \mathbb{N}(F_i) \setminus F_j} m_{F_k, F_i}^{old}(l_i) \right) \quad (3)$$

$$C_{F_i}(l_i) = E_{data}(F_i, l_i) \prod_{F_k \in \mathbb{N}(F_i)} m_{F_k, F_i}(l_i) \quad (4)$$

The symbol N defines the maximum of qualified view candidates to be assigned to a face, i.e., some faces may have less than N associated views after view selection, since 1) there may be no sufficient views for a specific face due to occlusion; 2) the final costs of some views are much larger than others', which may occur for the façades viewed by a limited number of "good" views but many "bad" views. For the second case, a ratio test is applied to eliminate the "bad" views: assume $c = c_1, c_2, \dots, c_N$ sorted in ascending order is the final costs of top N candidates $l = l_1, l_2, \dots, l_N$ for a specific face, candidates $\{l_i, \dots, l_N\}$ will be removed if $c_{i-1}/$

c_i is below a threshold (0.4 is used throughout our experiment as an empirical value).

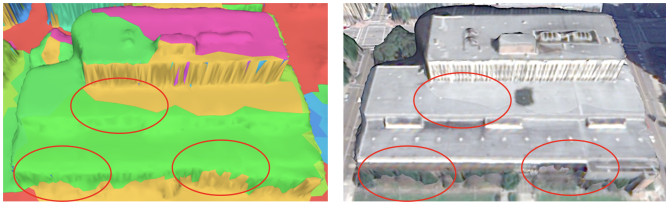


Fig. 3. Luminance differences existing in single (best) view based texture mapping. Left: One color represents a best view for each mesh face; Right: only the best view is assigned to map textures with no color adjustment. As highlighted in red circles, two observations are noted: 1) there are visible luminance differences between patches; 2) the façade near the ground is textured by two views with apparently different qualities, one is favored by the roof and the other is favored by the ground.

C. Multi-view blending based on distance transformation

There are multiple “good” views for each mesh face after the view selection procedure and there will still exist minor color differences among them. Direct fusion with equal weights for all involved views will cause color discontinuities and blurriness, especially for the faces whose top N views are different. We therefore introduce a modified alpha image blending algorithm based on distance transformation, as it was shown to be effective in image stitching applications. The algorithm consists of the following steps: Each face is assigned with N views and for each view, a mask consisting of all valid pixels (corresponding to the face and non-occluded) is firstly generated for the view (see examples of the mask highlighted in red in the first row of **Fig. 4 (a)**), followed by computing L^2 distance transform (see the second row of **Fig. 4 (a)**), the final texture for each face is obtained by blending all assigned view data together with associated distance transforms as weights (see **Fig. 4 (c)**). If assigning the single and best view to map the texture, as shown in **Fig. 4 (b)**, it will show apparent luminance differences, which can be greatly reduced by the proposed view blending approach (see **Fig. 4 (c)**).

IV. EXPERIMENTS

Our proposed method has been tested on three different types of datasets (Satellite dataset, unmanned-aerial vehicle (UAV) dataset, and close-range dataset) of varying complexity. Specific data parameters are listed in **Table IV**. All datasets are tested on a workstation with two 14-core Xeon W-2275 CPUs and 128 GB of memory. To demonstrate the effectiveness and efficiency of the proposed method, the proposed approach is variably compared against three SOTAs including both blending-based and MRF-based methods: (1) masked photo blending [9], which generates multiple masks per image, e.g. intersection angle, depth map border map, etc., then combine all masks into maps as weights for images in the final multi-view blending to yield the mesh texture. It is a classic blending-based TM method, which is simple and applicable for different types of camera models, used as a baseline in our experiments; (2) MVS (Multi-View Stereo)-based texture mapping [6] that builds on the MRF energy function to

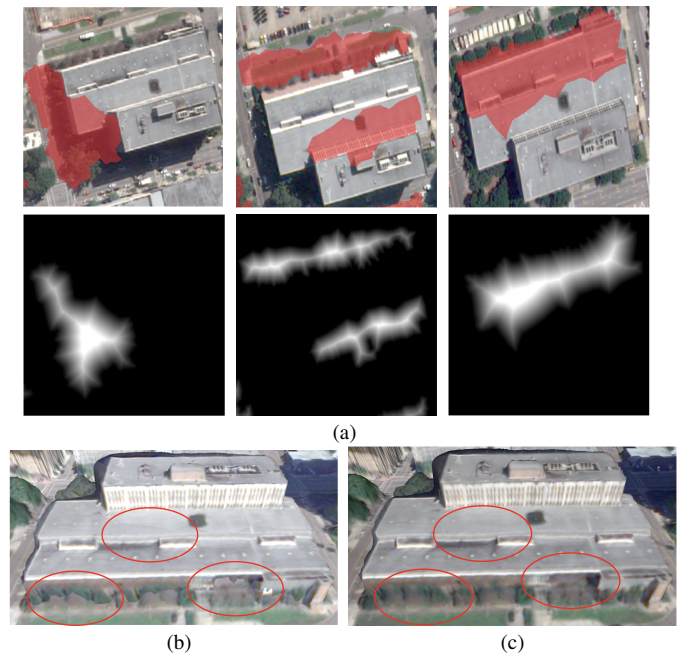


Fig. 4. Example depicting our view-blending approach. (a) first row: the masks for blending (highlighted in red); second row: their corresponding distance transformations, a higher value means a larger distance to the borders of the mask in the first row. (b) is a building with faces textured by merely the best view, similar to those with the graph-cut solution, while (c) is the view-blending result of the top three images. Regions highlighted in circles show significant improvements over seamlines between faces.

select an optimal view for each mesh face, followed by global color adjustment and Poisson editing [23] to minimize visible luminance difference between patches. Since it does not support RPC as a camera model and is designed for large-scale texturing, we use it as a comparison in the UAV dataset; (3) patch-based optimization for TM [8], which synthesizes aligned images from input images even with inaccurate camera poses by proposing a patch-based optimization system to avoid ghosting and blurring artifacts in the result. However, this method is not scalable (see **Section IV-C**), and thus it is only used in the close-range dataset. In addition, a well-known commercial photogrammetry software Metashape Pro [30] is also used in all three experiments to generate the mesh textures from input 3D mesh models and image data as a comparison, the algorithm of which is unknown.

We implemented our framework and Callieri et al.’s method [9] in C/C++ and used the authors’ code for Waechter et al. [6]. For Bi et al.’s approach [8], an available open-source implementation on GitHub [31] was used. We used default parameter configurations for all these compared approaches since these were tested to perform the best empirically. Specifically, in the MRF energy optimization, although as mentioned in Lempitsky and Ivanov’s work [7], the GC solver (i.e. α -expansion) achieves the best performance over the LBP solver, however, unlike the GC solver which cannot be parallelized easily due to the graph’s irregular structure, the LBP solver has been fully parallelized in our implementation, which yields greater resource use and computational efficiency.

The evaluations of these three datasets are performed in the following three subsections, where we performed both

TABLE I
SUMMARY OF THE THREE DATASETS.

dataset	#views	#mesh faces	source image dimension	orientation parameters	compared method
Satellite	12	1.9 million	42253 × 32125	RPC parameter after bundle adjustment	(1),(4)
UAV	113	2.4 million	5472 × 3648	Calibrated camera poses	(1),(2),(4)
Close-range	33	0.06 million	640 × 480	Camera poses	(1),(3),(4)

(1) Callieri et al.'s method [9]; (2) Waechter et al.'s method [6]; (3) Bi et al.'s method [8]; (4) Metashape Pro [30].

1) qualitative evaluation (visual comparison), 2) quantitative evaluation, and 3) running time and memory use. Most of the SOTAs evaluate their methods through either visual assessment or running time. As far as we know, there is no generally accepted method or indicator to measure the accuracy and reliability of the 3D texture. Thus, we designed a new texture quality assessment method, following the intuition that the rendered image from the textured model should coincide with the original image. Then, the difference between the rendered and the original image is assessed using the Peak signal-to-noise ratio (PSNR) and the multiscale structural similarity index measure (MS-SSIM) [32]. More specifically, for an input image I_i and its associated camera pose (or RPC for satellite data) pos_i , a virtual image V_i with the same resolution as I_i was firstly captured at pos_i from one textured result, and the image quality for generated V_i was then quantified in terms of some selected indicators (e.g. PSNR and MS-SSIM in our experiment) with respect to the original image I_i , these assessments were collected for all input images, the mean PSNRs and the mean MS-SSIMs were further computed over all assessments as quality indicators for the whole dataset. Note that, for both PSNR and MS-SSIM, the higher the value, the higher the image quality.

A. Experiment on the satellite dataset

Twelve 0.5m GSD (Ground Sampling Distance) WorldView I/II satellite images covering the main campus of the Ohio State University (OSU) in Columbus, Ohio, USA, are collected and processed using the satellite stereo processing software RSP [4] to generate the plain mesh for this region. Due to the large coverage and the high angular agility of the WorldView I/II satellites, all satellite images in the dataset cover the whole region at various angles (up to 15 degrees of off-nadir angle). An example is shown in **Fig. 5**, where a near nadir image contains minimal distortion on the roofs, but does not contain visible textures of the façades, while an off-nadir image contains visible façades with less optimal roof textures. Therefore, an independent per-face quality indicator will likely select **Fig. 5(a)** for façade textures and **Fig. 5(b)** for roofs, which inevitably causes seamlines. Our proposed approach, instead of selecting one of them, will take both and blend them to explore the advantages of both images, at the same time, create seamless texture mapping results across roof and façade boundaries.

TM for this region using the proposed method is completed within 4 minutes and consumed 4 GB peak memory, yielding a visually consistent textured mesh as shown in **Fig. 6**. Two other methods are used as a comparison: 1) Metashape Pro [30] and 2) Callieri et al.'s method [9].



Fig. 5. Two satellite images with different viewing angles. (a) shows an off-nadir image with visible façades; (b) shows primarily textures of roofs in a nearly nadir view.



Fig. 6. Examples of texture mapping results of the satellite dataset. Top: the overview of the textured mesh. Bottom: enlarged views to show details on façades.

Metashape Pro with its newest support for satellite datasets was applied to this dataset and the results are shown in **Fig. 7**. We observed that the textured mesh generated with default configurations reflected a large number of systematic errors. Since no warnings or errors were found in its log file, the authors perceive the results are not numerically comparable and potentially due to unknown system errors. Thus, it is not included for further qualitative comparison.

The comparisons of running time & memory use and quantitative evaluation are listed in **Table II**. Callieri's method used slightly fewer memories than ours, however, our method is faster, because Callieri's method requires computations in generating various weight maps for different quality indicators compared to our well-designed efficient data term, besides, its blending function involves all input images for each mesh face, while ours only blends the selected top N views. In addition, two quantitative indicators, i.e. the mean PSNR and mean MS-SSIM over the entire test dataset, show that the textured results

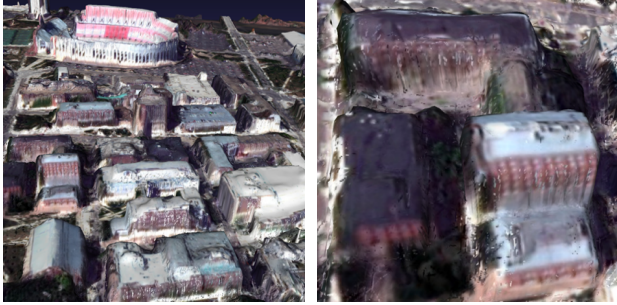


Fig. 7. Some texturing results from Metashape Pro. White noises can be seen everywhere.

generated from both Callieri's blending-based TM method and ours have comparable quality, while ours uses fewer and highly selective views.

TABLE II

RUNNING TIME & PEAK MEMORY AND QUANTITATIVE EVALUATION FOR DIFFERENT TM METHODS APPLIED TO THE SATELLITE DATASET.

	Running time (sec)	Peak memory usage (GB)	Mean PSNR	Mean MS-SSIM
Callieri et al.	270	3.79	16.26	0.60
Ours	232	3.84	16.35	0.61

Visual comparisons of different methods are shown in **Fig. 8**, including 1) a best-view selection method for TM **Fig. 8(b)**, 2) Callieri's method **Fig. 8(c)**, and 3) ours **Fig. 8(d)**. It can be seen that the result using only the best view yields color differences among triangles, while both Callieri's method and ours show consistent texture rendering. Ours **Fig. 8(d)** shows apparently sharper texture rendering as compared to Callieri's method, since our method uses the top-N views with optimal quality selected through the MRF framework, while Callieri's method simply blends all views, which yields reduced and blurred texture.

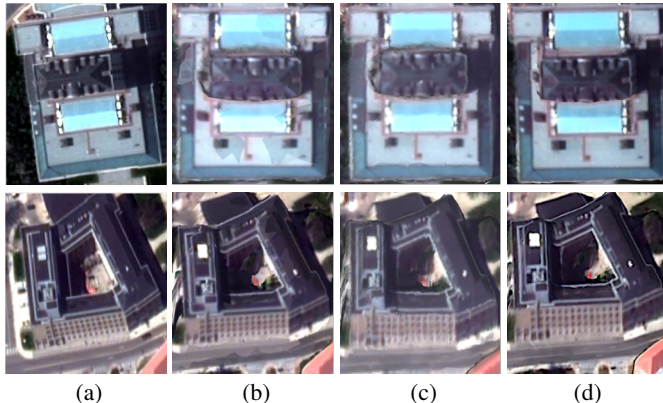


Fig. 8. Two examples for view blending. (a) Original image; (b) rendered view using a best view selection algorithm; (c) rendered view of Callieri's method [9]; (d) ours.

B. Experiment on the UAV dataset

The UAV dataset consists of 113 images covering an area mixed with buildings and fields, published by senseFly [33].

We used OpenMVG [34] to adjust all input camera poses, followed by using OpenMVS to generate the plain mesh. We applied our proposed method to produce the textured mesh compared against three SOTAs, i.e. 1) Callieri et al.'s [9], 2) Waechter et al.'s [6] and 3) Metashape Pro [30]. The evaluation includes visual comparison, quantitative texture assessment and running time & memory usage. The overviews for all textured results are illustrated in **Fig. 9**, where it can be seen that these textured models are generally of good quality. However, Waechter et al.'s introduces artifacts highlighted in red rectangles may due to its extra global seam leveling.

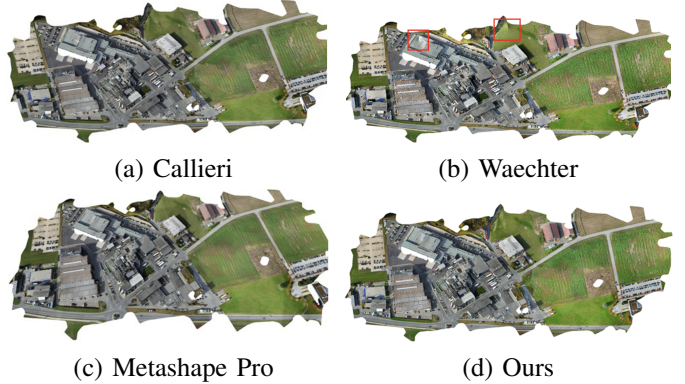


Fig. 9. Overviews for four textured meshes from (a) Callieri et al.'s method [9]; (b) Waechter et al.'s method [6]; (c) Metashape Pro [30]; (d) our proposed method. The results look similar to each other except Waechter et al.'s has some artifacts highlighted in red rectangles.

The running time & peak memory for all methods are shown in **Table III** except for the Metashape Pro since it is a black-box and interactive software. Callieri et al.'s method consumes more computations in weight map generation and image blending (as mentioned in **Section IV-A**), thus it incurs more computation time. The total running time for Waechter et al.'s method is 20 minutes, while ours is 16 minutes, roughly 20% more efficient. For peak memory usage, Waechter et al.'s method is 12.82 GB while ours is 16.10 GB. Our method uses marginally more memories mainly due to two strategies: 1) fully parallelized LBP solver instead of GC solver in MRF energy optimization, 2) top N views are stored in memory in preparation for the image blending algorithm. Quantitative evaluation in **Table III** shows the indicators computed from ours are slightly higher than all three other methods' on the whole dataset, which indicates the proposed method is able to render textures closer to the input image quality than other methods.

TABLE III
RUNNING TIME & PEAK MEMORY AND QUANTITATIVE EVALUATION FOR DIFFERENT TM METHODS APPLIED TO THE UAV DATASET.

	Running time (min)	Peak memory usage (GB)	Mean PSNR	Mean MS-SSIM
Callieri et al.	26	14.52	16.48	0.54
Waechter et al.	20	12.82	15.87	0.61
Metashape Pro	N.A.	N.A.	16.49	0.50
Ours	16	16.10	16.76	0.64

Fig. 10 gives three different examples of enlarged views where three SOTAs all produced poor texturing results, e.g.

visible seamlines and noises, tearing and discoloration. Some issues (i.e. seamline and tearing) are caused by the corresponding blending algorithm. For example, Callieri et al.'s method blends all candidate images, in which poor images saturated "good" ones, resulting in blurry and inconsistent textures (first row of **Fig. 10**). Areas with too few "good" views are also problematic, as the best-view selection algorithm might not accurately select the real "best" one. For example, we observe from the result of Waechter et al.'s method (second row of **Fig. 10**), the façade textures are not necessarily of the best quality, as it was geared towards having the same view as neighboring faces, which in this case are roof faces, thus using the same view as used by the roof faces result in the loss of resolution. In addition, although no technical details about its TM algorithm are known for Metashape Pro, it yielded a high-quality texture except for some apparent artifacts that may be due to over color adjustment (third row of **Fig. 10**). However, our proposed method is less problematic for all these issues, as it leverages "good" views not only on each face, but also across neighboring faces during weighted blending (last row of **Fig. 10**).



Fig. 10. Three examples of difficult texturing regions showing our advantages over other three methods: Callieri et al.'s method [9], Waechter et al.'s method [6], Metashape Pro [30]. First row: visible seamline and noises; Second row: poor texturing faces and over color adjustment; Third row: carving artifacts; Last row: seamless high-quality texture.

Since our proposed method in nature blends multiple views, it is still inherently affected by inaccuracies of either the geometry or camera poses, as shown in **Fig. 11**, where these single-view methods apparently achieved better results, and although our result shows ghosting effects, it still outperforms the other blending-based method (e.g. Callieri et al.).

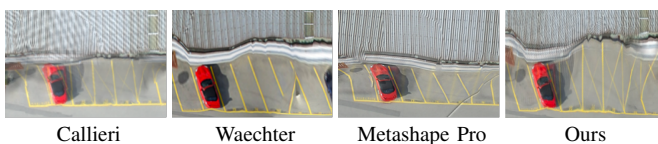


Fig. 11. An example showing drawbacks in the proposed methods at its ghosting artifacts due to inaccurate geometry/camera poses.

In conclusion, our proposed method can generate the mesh

texture in slightly better quality than other SOTAs, and consume less computation (i.e. 20% faster), overcome several artifacts found in Callieri's, Waechter's and Metashape Pro. However, ghosting artifacts is a remaining challenge in our future work.

C. Experiment on the close-range dataset

The Fountain scene from Zhou and Koltun [35] is used to discuss the limitations of our proposed method. Since the plain mesh was already provided along with 33 images, we directly tested the proposed method against three SOTAs, i.e. 1) Callieri's method [9], 2) Bi's method [8] and 3) Metashape Pro [30], in three aspects: (1) running time & peak memory usage; (2) quantitative evaluation and (3) visual check. The overviews for all textured results are illustrated in **Fig. 12**, where we can see all four methods have their own limitations, such as Callieri's and ours are blurrier than the other two's, especially for the texts in the middle. Bi's has missing parts near borders because the number of visible views for that regions don't meet its requirement, and Metashape Pro's has apparently tearing as highlighted in **Fig. 12(c)**.

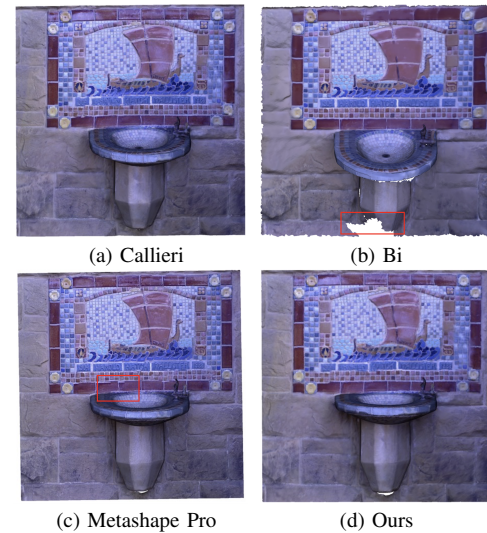


Fig. 12. Overviews for four textured meshes from (a) Callieri et al.'s method [9]; (b) Bi et al.'s method [8]; (c) Metashape Pro [30]; (d) our proposed method. Callieri's and ours are similar to each other and are both blurrier than the other two methods (see the texts in the middle of pictures). However, there is apparently tearing in Metashape Pro's result as highlighted in rectangle and Bi's result, although with fewer artifacts, has missing parts near borders.

As a performance comparison listed in **Table IV**, it costs only 24 seconds and 193 MB memories for the proposed method to generate the textured mesh, faster than Callieri's method, the same as in previous experiments, while Bi's method consumed 120 MB memories and took over 1 hour to generate results, two orders of magnitude slower than ours, proven to be not-applicable for TM of large dataset. **Table IV** shows that all the quantitative measures are lower than those in the previous experiments, which implies the challenge of this dataset, which may be due to inaccurate input camera poses and strong illumination and exposure differences exhibited in the input images. Our method is the fastest among the compared methods and achieves the second best result in

texture measure (only marginally worse than the Metashape Pro).

TABLE IV

RUNNING TIME & PEAK MEMORY AND QUANTITATIVE EVALUATION FOR DIFFERENT TM METHODS APPLIED TO THE CLOSE-RANGE DATASET.

	Running time (sec)	Peak memory usage (MB)	Mean PSNR	Mean MS-SSIM
Callieri et al.	39	207	12.42	0.31
Bi et al.	>3600	120	12.76	0.38
Metashape Pro	N.A.	N.A.	12.84	0.39
Ours	24	193	12.78	0.38

We note that these inherent challenges, especially the inaccurate camera poses, lead to slight blurring and ghosting artifacts, even distortions in the final texture for our proposed method (see **Fig. 13**). However, when checking details against the other three results, although ours has a little more distortions and is slightly blurrier than Metashape Pro's and Bi's, our result is overall reasonable and acceptable, especially considering its efficiency and capability to process other types of datasets as well.

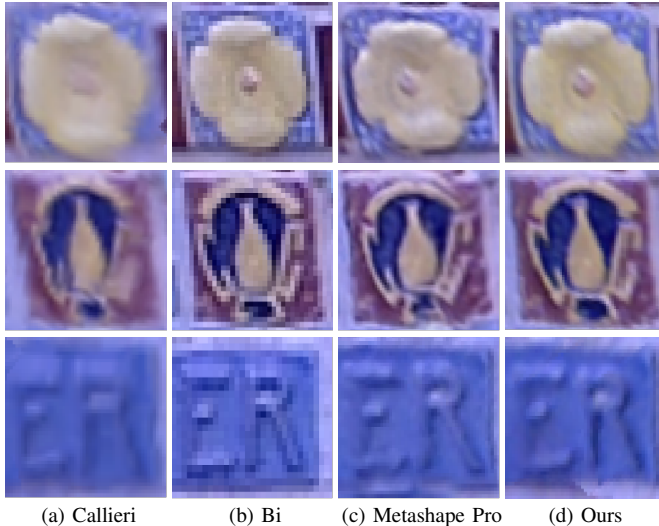


Fig. 13. Visual comparison for four texture mapping results on the close-range dataset: (a) Callieri et al.'s result [9]; (b) Bi et al.'s result [8]; (c) Metashape Pro's result [30]; and (d) ours. Ours is blurrier than Bi et al.'s and Metashape Pro's due to multi-view blending with inaccurate camera poses, but is better than Callieri et al.'s. For Bi et al.'s, although no blurring or ghosting artifacts are found, seems to have a lower resolution than Metashape Pro's, which has the highest quality texture with more details.

V. CONCLUSION

Typical texture mapping algorithms for aerial photogrammetry applications are designed to process regular images collected under consistent lighting conditions. However, this presents a challenge when these algorithms are scaled to process multi-view and large-frame images, where a large number of large-sized images under drastically different lighting conditions brings about a highly non-linear image intensity difference and order-of-magnitude number of faces to optimize. In this paper, we present a novel texture mapping framework for large-scale 3D reconstructions, which are able to achieve better accuracy

as well as efficiency than other SOTAs across both space-borne and aerial-borne platforms, due to:

- 1) **Top-N best views instead of “one-best-view”.** Typical MRF-based methods find the “one-best-view”, which may select suboptimal views for mesh faces without chances to correct, i.e. it is impossible to leverage texture fusion algorithms once it is set. This is typically problematic for high-altitude images. When selecting views for faces connecting the roof and the façade of a building, such algorithms would often select a single suboptimal view for the façade, in order to favor spatial smoothness constraints, and result in distorted textures. However, ours produces the top-N best views per face, giving an additional chance to perform post-patch-fusion for conflicting view selections. In this case, ours can achieve high-quality textures for both roof and façade faces, as evidenced by **Section IV-A**.
- 2) **More general data term.** We provide a more general data term designated to support more objectives and generic enough to support multiple camera models (e.g. camera poses and RPCs as well). This provides an important feature when using both satellite images and aerial/UAV images to generate texture from combined sources.
- 3) **Simple and efficient image blending algorithm.** We discard the typical complex post color correction scheme, and instead use a local blending scheme to minimize seamlines. This is not regarded as a compromise, but a benefit from the selection of N views instead of one. It provides much more flexibility for an efficient image blending algorithm to achieve color consistency without additional color correction, and preserves the original input texture to the greatest extent as well.
- 4) **Fully parallelized LBP solver.** In the MRF energy optimization, the GC solver is the most widely used solver due to its best performance over other solvers on a single CPU core. However, unlike the GC solver which cannot be parallelized easily due to the graph's irregular structure, the LBP solver has been fully parallelized in our implementation, which yields greater resource use and computational efficiency.

The proposed method is evaluated with three typical datasets: a wide-area satellite dataset (covering 4 km^2), a UAV dataset containing over 100 images and a close-range dataset named “Fountain”. We compared our proposed method with four SOTAs through (1) visual quality check; (2) quantitative assessment; (3) running time performance evaluation. Experimental results show that the proposed method achieves textured meshes with more consistent and high-resolution texture, even in very difficult scenarios such as faces connecting façades and roofs. At the meantime, it is at least 20% faster than all the other methods with only a slightly increased memory use. Moreover, among all these tested methods, our method consistently achieves reasonable results across the tested dataset, and is shown as the only one achieving a visually pleasant result in the satellite dataset. Therefore, it is flexible and scalable to handle all the tested scenarios at

different ranges of resolution and scene complexity. During our evaluation, we also observed that, since our method relies on multiple views, it may yield a slightly blurry texture for inaccurate geometry and camera poses. Thus, our future effort will focus on adaptively determining the number of views to use during TM to address this challenge.

VI. ACKNOWLEDGMENTS

This work is partially supported by Office of Naval Research (Award No. N000141712928 & N000142012141). We thank SenseFly for making the drone dataset available and thank Debao Huang for his assistance in running part of the experiments.

REFERENCES

- [1] A. Gruen, G. Schrotter, S. Schubiger, R. Qin, B. Xiong, C. Xiao, J. Li, X. Ling, and S. Yao, “An Operable System for LoD3 Model Generation Using Multi-Source Data and User-Friendly Interactive Editing: Final Report,” ETH Zurich, Report, 2020, accepted: 2020-04-14T08:54:52Z. [Online]. Available: <https://www.research-collection.ethz.ch/handle/20.500.11850/409483>
- [2] L. Hoegner and U. Stilla, “Automatic 3D reconstruction and texture extraction for 3D building models from thermal infrared image sequences,” *Quant. InfraRed Thermogr.*, 2016.
- [3] G. Guidi, M. Russo, S. Ercoli, F. Remondino, A. Rizzi, and F. Menna, “A Multi-Resolution Methodology for the 3D Modeling of Large and Complex Archeological Areas,” *International Journal of Architectural Computing*, vol. 7, no. 1, pp. 39–55, Jan. 2009, publisher: SAGE Publications. [Online]. Available: <https://doi.org/10.1260/147807709788549393>
- [4] R. Qin, “Rpc stereo processor (RSP)—a software package for digital surface model and orthophoto generation from satellite stereo imagery,” *International Archives of the Photogrammetry, Remote Sensing & Spatial Information Sciences*, vol. 3, p. 77, 2016, publisher: Copernicus GmbH.
- [5] —, “Automated 3D recovery from very high resolution multi-view images Overview of 3D recovery from multi-view satellite images,” in *ASPRS Conference (IGTF) 2017*, 2017, pp. 12–16.
- [6] M. Waechter, N. Moehrle, and M. Goesele, “Let there be color! Large-scale texturing of 3D reconstructions,” in *European conference on computer vision*. Springer, 2014, pp. 836–850.
- [7] V. Lempitsky and D. Ivanov, “Seamless mosaicing of image-based texture maps,” in *2007 IEEE conference on computer vision and pattern recognition*. IEEE, 2007, pp. 1–6.
- [8] S. Bi, N. K. Kalantari, and R. Ramamoorthi, “Patch-based optimization for image-based texture mapping,” *ACM Trans. Graph.*, vol. 36, no. 4, pp. 1–11, Jul. 2017. [Online]. Available: <https://dl.acm.org/doi/10.1145/3072959.3073610>
- [9] M. Callieri, P. Cignoni, M. Corsini, and R. Scopigno, “Masked photo blending: Mapping dense photographic data set on high-resolution sampled 3D models,” *Computers & Graphics*, vol. 32, no. 4, pp. 464–473, Aug. 2008. [Online]. Available: <https://www.sciencedirect.com/science/article/pii/S009784930800054X>
- [10] C. Yanover and Y. Weiss, “Finding the M most probable configurations using loopy belief propagation,” *Advances in neural information processing systems*, vol. 16, pp. 289–296, 2003, publisher: Citeseer.
- [11] V. Kolmogorov and R. Zabin, “What energy functions can be minimized via graph cuts?” *IEEE Transactions on Pattern Analysis & Machine Intelligence*, vol. 26, no. 2, pp. 147–159, 2004, publisher: IEEE.
- [12] Y. Boykov and O. Veksler, “Graph Cuts in Vision and Graphics: Theories and Applications,” in *Handbook of Mathematical Models in Computer Vision*, N. Paragios, Y. Chen, and O. Faugeras, Eds. New York: Springer-Verlag, 2006, pp. 79–96. [Online]. Available: http://link.springer.com/10.1007/0-387-28831-7_5
- [13] S. Z. Li, “Markov random field models in computer vision,” in *Computer Vision — ECCV '94*, ser. Lecture Notes in Computer Science, J.-O. Eklundh, Ed. Berlin, Heidelberg: Springer, 1994, pp. 361–370.
- [14] M. Xu, H. Chen, and P. K. Varshney, “An image fusion approach based on markov random fields,” *IEEE Transactions on Geoscience and Remote Sensing*, vol. 49, no. 12, pp. 5116–5127, 2011.
- [15] L. Grammatikopoulos, I. Kalisperakis, G. Karras, and E. Petsa, “Automatic multi-view texture mapping of 3D surface projections,” in *Proceedings of the 2nd ISPRS International Workshop 3D-ARCH*. Citeseer, 2007, pp. 1–6.
- [16] C. Allene, J.-P. Pons, and R. Keriven, “Seamless image-based texture atlases using multi-band blending,” in *2008 19th International Conference on Pattern Recognition*, Dec. 2008, pp. 1–4, iSSN: 1051-4651.
- [17] A. Baumberg, “Blending Images for Texturing 3D Models.” in *Bmvc*, vol. 3. Citeseer, 2002, p. 5.
- [18] Y. Li and L. Ma, “A fast and robust image stitching algorithm,” in *2006 6th world congress on intelligent control and automation*, vol. 2. IEEE, 2006, pp. 9604–9608.
- [19] R. Szeliski, “Image alignment and stitching,” in *Handbook of mathematical models in computer vision*. Springer, 2006, pp. 273–292.
- [20] R. Gal, Y. Wexler, E. Ofek, H. Hoppe, and D. Cohen-Or, “Seamless Montage for Texturing Models,” *Computer Graphics Forum*, vol. 29, no. 2, pp. 479–486, 2010, _eprint: <https://onlinelibrary.wiley.com/doi/pdf/10.1111/j.1467-8659.2009.01617.x> [Online]. Available: <https://onlinelibrary.wiley.com/doi/abs/10.1111/j.1467-8659.2009.01617.x>
- [21] Y. Fu, Q. Yan, L. Yang, J. Liao, and C. Xiao, “Texture mapping for 3d reconstruction with rgb-d sensor,” in *Proceedings of the IEEE conference on computer vision and pattern recognition*, 2018, pp. 4645–4653.
- [22] W. Li, H. Gong, and R. Yang, “Fast texture mapping adjustment via local/global optimization,” *IEEE transactions on visualization and computer graphics*, vol. 25, no. 6, pp. 2296–2303, 2018, publisher: IEEE.
- [23] P. Pérez, M. Gangnet, and A. Blake, “Poisson image editing,” in *ACM SIGGRAPH 2003 Papers*, 2003, pp. 313–318.
- [24] D. Cernea, “Openmvs: Open multiple view stereovision,” 2015. [Online]. Available: <https://github.com/cdcseacave/openMVS>
- [25] V. Kolmogorov, “Convergent tree-reweighted message passing for energy minimization,” in *International Workshop on Artificial Intelligence and Statistics*. PMLR, 2005, pp. 182–189.
- [26] R. Fabbri, L. D. F. Costa, J. C. Torelli, and O. M. Bruno, “2D Euclidean distance transform algorithms: A comparative survey,” *ACM Computing Surveys (CSUR)*, vol. 40, no. 1, pp. 1–44, 2008, publisher: ACM New York, NY, USA.
- [27] C. Buehler, M. Bosse, L. McMillan, S. Gortler, and M. Cohen, “Unstructured lumigraph rendering,” in *Proceedings of the 28th annual conference on Computer graphics and interactive techniques*, ser. SIGGRAPH '01. New York, NY, USA: Association for Computing Machinery, Aug. 2001, pp. 425–432. [Online]. Available: <https://doi.org/10.1145/383259.383309>
- [28] G. Zhou, X. Bao, S. Ye, H. Wang, and H. Yan, “Selection of optimal building facade texture images from uav-based multiple oblique image flows,” *IEEE Transactions on Geoscience and Remote Sensing*, vol. 59, no. 2, pp. 1534–1552, 2021.
- [29] N. Greene, M. Kass, and G. Miller, “Hierarchical Z-buffer visibility,” in *Proceedings of the 20th annual conference on Computer graphics and interactive techniques*, 1993, pp. 231–238.
- [30] A. LLC., “Metashape pro,” Aug. 2021. [Online]. Available: <http://www.agisoft.com>
- [31] Eagle, “EAGLE-TextureMapping,” Aug. 2021, original-date: 2019-09-10T08:52:25Z. [Online]. Available: <https://github.com/OneEyedEagle/EAGLE-TextureMapping>
- [32] Z. Wang, E. P. Simoncelli, and A. C. Bovik, “Multiscale structural similarity for image quality assessment,” in *The Thirty-Seventh Asilomar Conference on Signals, Systems & Computers*, 2003, vol. 2. Ieee, 2003, pp. 1398–1402.
- [33] senseFly, “Discover a wide range of drone datasets,” 2021. [Online]. Available: <https://www.sensefly.com/education/datasets/>
- [34] P. Moulon, P. Monasse, R. Perrot, and R. Marlet, “Openmvg: Open multiple view geometry,” in *International Workshop on Reproducible Research in Pattern Recognition*. Springer, 2016, pp. 60–74.
- [35] Q.-Y. Zhou and V. Koltun, “Color Map Optimization for 3D Reconstruction with Consumer Depth Cameras,” *ACM Transactions on Graphics*, vol. 33, Aug. 2014.